Faraday Discussions

Accepted Manuscript

This manuscript will be presented and discussed at a forthcoming Faraday Discussion meeting. All delegates can contribute to the discussion which will be included in the final volume.

Register now to attend! Full details of all upcoming meetings: http://rsc.li/fd-upcoming-meetings

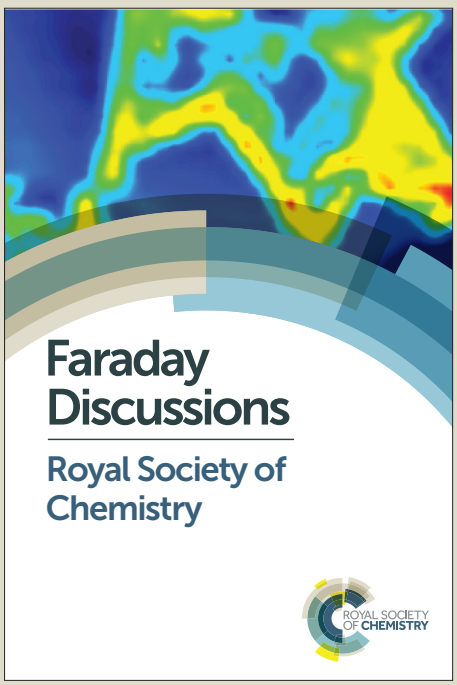

This is an *Accepted Manuscript*, which has been through the Royal Society of Chemistry peer review process and has been accepted for publication.

Accepted Manuscripts are published online shortly after acceptance, before technical editing, formatting and proof reading. Using this free service, authors can make their results available to the community, in citable form, before we publish the edited article. We will replace this *Accepted Manuscript* with the edited and formatted *Advance Article* as soon as it is available.

You can find more information about *Accepted Manuscripts* in the Information for Authors.

Please note that technical editing may introduce minor changes to the text and/or graphics, which may alter content. The journal's standard Terms & Conditions and the Ethical guidelines still apply. In no event shall the Royal Society of Chemistry be held responsible for any errors or omissions in this *Accepted Manuscript* or any consequences arising from the use of any information it contains.

ROYAL SOCIETY OF CHEMISTRY

www.rsc.org/faraday_d

Breaking the simple proportionality between molecular conductances and charge transfer rates

Ravindra Venkatramani, [†,‡,*] *Emil Wierzbinski,* [§] *David H. Waldeck,* [§,*] *and David N. Beratan* [‡,¶,*]

[†]Department of Chemical Sciences, Tata Institute of Fundamental Research, Homi Bhabha Road, Colaba, Mumbai 400 005, India

[‡]Department of Chemistry, Duke University, Durham, NC, 27708, USA

[§]Department of Chemistry, University of Pittsburgh, Pittsburgh, PA, 15260, USA

[¶]Departments of Biochemistry and Physics, Duke University, Durham, NC, 27708, USA

*corresponding authors

Abstract

A theoretical framework is presented to describe and to understand the observed relationship between molecular conductances and charge transfer rates across molecular bridges as a function of length, structure, and charge-transfer mechanism. The approach uses a reduced density matrix formulation with a phenomenological treatment of system-bath couplings to describe charge-transfer kinetics and a Green's function based Landauer-Buttiker method to describe steady-state currents. Application of the framework is independent of the transport regime and includes bath-induced decoherence effects. This model shows that the relationship between molecular conductances and charge transfer rates follows a power-law. The nonlinear rate-conductance relationship is shown to arise from differences in the charge transport barrier heights and from differences in environmental decoherence rates for the two experiments. This model explains otherwise puzzling correlations between molecular conductances and electrochemical kinetics.

Keywords: charge transport, molecular junction, electrochemical rate constant, molecular bridge, decoherence, superexchange, thermal hopping

The last decade has witnessed a growing interest in understanding the relationship between charge transfer (CT) kinetics and molecular conductance.[1-4] A substantial literature exists for unimolecular CT rates in donor-bridge-acceptor (D-B-A) structures comprised of charge donor (D) and acceptor (A) moieties that are connected by a bridging molecular unit (B).[5-9] In addition, the chemical donor and acceptor groups may be replaced with electrodes (M) to measure unimolecular electrochemical CT rates[10-13] and molecular conductances. [14-19] One expects unimolecular CT rates, molecular conductances, and electrochemical rates to be linked because the conduit (bridge) for charge transmission can be made chemically identical in the different experiments. Yet, recent experimental studies find fundamental differences among the transport characteristics in these experiments, and these differences may lead to nonlinear relationships among the measured quantities.[20]

Nitzan highlighted the fundamental connection between steady-state CT rates in D-B-A systems and their molecular conductances over a decade ago.[21, 22] He proposed a linear relationship between the nonadiabatic, unimolecular CT rate constant in D-B-A structures and the zero bias molecular conductance in M-B-M junctions, assuming identical molecular bridges and a superexchange CT mechanism.[1] Subsequently, he described hopping CT through structures with identical repeating bridging units, and found a similar linear correlation between CT rates and molecular conductances for long bridges with high tunneling barriers.[2] Berlin and Ratner extended that treatment to the hopping CT regime with more general molecular bridge models, while retaining the large-barrier assumption.[3] In an alternative approach, Lewis and coworkers used Fermi's golden rule to relate unimolecular CT rates (in D-B-A molecules), electrochemical rate constants (in M-B-A assemblies), and molecular conductances (in M-B-M junctions),[4] treating the donor-acceptor electronic coupling as a parameter. For D-B-A systems, the CT was assumed to occur between a single electronic state of the donor and a single electronic state on the acceptor; for M-B-A and M-B-M systems, the CT was allowed to occur between multiple electronic states on the electrode and a molecular acceptor (M-B-A), or with multiple electronic states on a second electrode (M-B-M). If each electronic state on an electrode is considered analogous to the single state on the donor/acceptor molecule, then CT across M-B-A/M-B-M junctions can be described by an effective electronic coupling per electronic state times a density-of-states factor for the electrodes. Assuming that the D-B-A electronic coupling is equal to the M-B-A/M-B-M electronic coupling per charge carrying state of the electrode, Traub *et al.*

predicted the resistances of M-B-M structures based on available CT rate data for alkanethiolate, oligophenylene, and DNA bridges in D-B-A or M-B-A experiments.[4] Each of these earlier studies[1-4] predicted a linear correlation between the tunneling or hopping CT rate and the conductance for a high barrier molecular bridge. Yet experiments indicate that molecular conductances and CT rates do not satisfy simple linear correlations (*vide infra*, ref. 20).

Fig. 1 plots experimental conductances (obtained from scanning tunneling microscope-controlled break junction (STM-BJ) experiments) versus electrochemical CT rates for the same molecular bridges.[20] In all cases, molecules were attached (at both ends in the conductance experiments and at one end in the electrochemical experiments) to the gold electrode through thiol linkers. In the electrochemical experiments, ferrocene tethered to the molecule's free

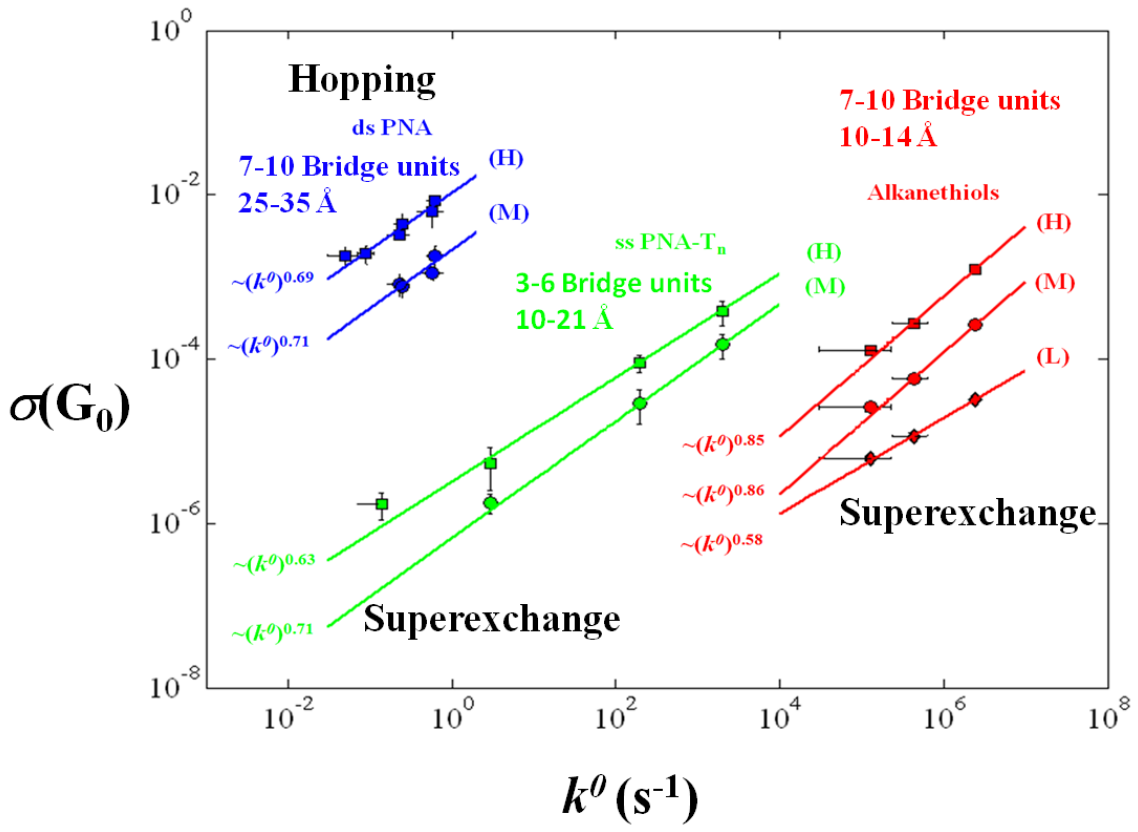

Figure 1. Dependence of the single molecule conductance σ on the electrochemical charge transfer rate constant k^0 for alkanes (red symbols), ss PNA constructed of thymine nucleotides (ss PNA-T_n; n = 3 – 6) (green symbols), and ds PNAs (blue symbols). Lines represent the least squares fits in the form σ=A×$(k^0)^m$. Electrochemical rate constant values are adapted from Ref. 10 for alkanethiols, and Refs. 11 and 12 for ss PNAs. Conductance values for alkanedithiols are adapted from Ref. 19. Note that the same type of linker was used to attach the ss- and ds PNA molecules to the gold surface (Cys), whereas the alkyl chains are directly coupled to gold with thiol groups, rather than cysteines. In conductance measurements, several values of single-molecule conductance were determined for each molecule, dependent on details of the Au-S covalent bond geometry. H, M, and L represent respectively high, medium, and low families of reported conductances. Figure adapted from Ref. 20.

terminus was used as a redox reporter for rate measurements. Data are presented for three families of bridges: i) alkanes, ii) single stranded peptide nucleic acids (ss PNA), and iii) double stranded peptide nucleic acids (ds PNA). For each of the three families of bridges, the conductance and rate data are plotted as a function of bridge lengths. These data reveal two dramatic features that are at odds with previous theoretical predictions.[1-4] First, the conductance-rate data for each type of bridge is best fit by a power law relationship of the form: $\sigma \propto (k^0)^m$. Assuming that each measurement decays exponentially with distance ($k^0 \propto \exp(-\beta_{k^0} \times L)$ and $\sigma \propto \exp(-\beta_\sigma \times L)$), the exponent is $m=\beta_\sigma/\beta_{k^0}$.[20] Thus, a linear correlation between rates and conductances is recovered only when $\beta_\sigma = \beta_{k0}$. However, m values that are extracted from the data in Fig 1 range between ~ 0.6 – 0.9 for alkanethiols and between ~0.6-0.7 for the nucleic acid bridges.[20] Second, the value of m is not transferrable for rate-conductance relationships among different molecular bridges. For example, 7-10 base pair ds PNA (~25-35 Å length) shows both lower CT rates and higher molecular conductances than 10-18 Å ss PNA sequences and 10-14 Å alkane chains. In this manuscript we develop a theoretical framework to identify the physical parameters governing the complex rate-conductance relationship shown in Fig. 1.

Because previous theoretical models[1-4] predict a linear correlation between CT rate and molecular conductance, assumptions inherent to the models must be violated for the data in Fig. 1. First, the expressions in Ref. 1-4 were derived for specific mechanisms of charge transport, *i.e.*, superexchange [1, 4] or incoherent hopping with large donor/electrode-to-bridge energy gaps.[2, 3] In general, CT may include admixtures from different coherent mechanisms as well as from incoherent variable-range hopping and nearest neighbor hopping.[23-25] Indeed, recent studies with nucleic acids (PNA, DNA) found that a mixture of charge-transport mechanisms operate as a consequence of thermal fluctuations of the structures.[25] Another simplifying assumption used in deriving the expressions in Ref. 1-4 is that the CT energy barriers are equal (i.e., the energy gaps between charge carrying states on the bridge and those on the donor/acceptor/electrode are equal) for D-B-A/M-B-A structures and for M-B-M junctions. Because the CT energy barrier is a crucial determinant of CT mechanism(s), different CT barriers in conductance and rate measurements can lead to different CT mechanisms, or their admixtures. Third, the measurements are performed under different environmental conditions. That is, D-B-A rates are measured in solution, M-B-A rates are measured at electrochemical interfaces, and M-B-M conductances are measured in molecular junctions. These different environments can lead to

differences in the relaxation rates for populations and coherences of the bridge states. Thus, even if the molecular bridge retains the same conformation and electronic structure in the different settings, differences in the molecule-bath interactions and differences in the energies of donor/electrode charge states could cause deviations from a linear conductance-rate relationship. These effects are examined in the models developed here.

Describing mixed mechanism charge-transport is challenging, and general theoretical expressions that link unimolecular charge-transfer rates with steady state molecular conductances arising from mixed mechanisms do not yet exist. Reduced density matrix approaches to calculate charge-transfer rates, including bath-induced decoherence, were formulated by several groups.[21, 26, 27] The theoretical rates may be linked to unimolecular CT rates measured in experiments[27] when excess charge population on the bridge is negligible (i.e., for large tunneling barriers). A recent study by Yeganeh *et al*. describes an approach to calculate steady-state non-adiabatic CT rates in the framework of non-equilibrium Green's functions, which are typically used to calculate molecular conductances.[28] This approach is appealing, as it enables the description of steady-state non-adiabatic CT rates and conductances in one formalism; however, the bridge is not explicitly treated in the prescription and the approach cannot be used to describe transient CT kinetics in D-B-A or M-B-A structures. In the present study, the molecular conductance through a bridge is modeled in a Green`s function based Landauer-Buttiker framework, and the transient unimolecular CT rate (and the electrochemical rate constant) is treated with an initial value formulation of the density matrix. The framework presented here allows the computation of rate-conductance relationships for molecular bridges of different lengths, for different chemical species, and for mixed CT mechanisms. Our model calculations find that different CT energy barriers and different bath-induced decoherence effects (for molecular conductance versus CT rates) can produce nonlinearities in the rate-conductance relationships. These effects are not included in earlier theoretical studies of the link between rate and conductance,[1-4] which therefore predict linear correlations. The theoretical framework developed here helps to rationalize the complex relationship between the experimental rate and conductance data shown in Fig. 1.

Theoretical Models

We aim to establish a framework for calculating CT rates and molecular conductance with a minimum number of transferable parameters. The computational approach is structured to be independent of the charge-transfer mechanism and can incorporate bath-induced decoherence. For both rate and conductance calculations, the bridge is represented with a tight-binding Hamiltonian (H_{BR}). There are N identical repeat units in the bridge with equal site energies (E_B) and equal nearest-neighbor couplings (t_B):

$$\widehat{H}_B = \sum_{m=1}^{N} |m > E_B < m| + \sum_{m=1}^{N-1} |m > t_B < m+1| + |m+1 > t_B < m| \qquad (1)$$

As shown in Fig. 2, the tight binding bridge (green lines) is then either coupled to molecular donor-acceptor sites with nearest neighbor couplings (t_{D1} / t_{NA} terms in Fig. 2A) for CT rate calculations, or to donor-acceptor electrodes represented through renormalized complex broadening matrices (Γ_{L1} / Γ_{NR}). We next describe how the schemes in Fig. 2 can be used to describe unimolecular charge transfer rates, electrochemical rate constants, and molecular conductances. The theoretical approach presented here can be extended to more elaborate model structures and Hamiltonians.

Expression for the Charge Transfer Rate:

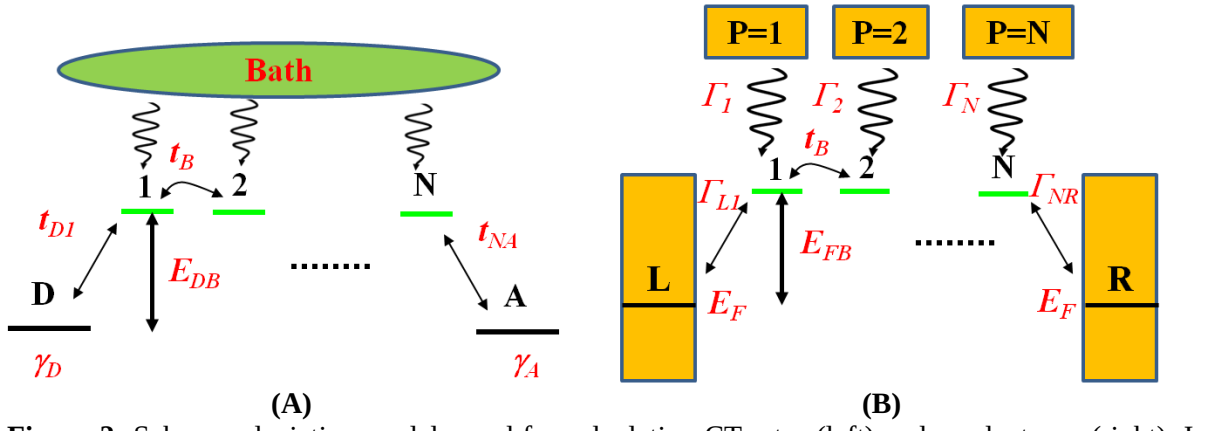

(A) (B)

Figure 2: Schemes depicting models used for calculating CT rates (left) and conductance (right). In both models, the bridge is defined by tight binding couplings t_{ij} and equal site energies E_B. The bridge is coupled (couplings t_{D1} / t_{NA}) to donor/acceptor sites (energies E_D = E_A) in the CT rate model and to electrodes (couplings Γ_{L1} / Γ_{NR}) of Fermi energy E_F in the conductance model. The CT energy barriers are given by E_{DB} = E_B – E_D and E_{FB} = E_B – E_F in the CT rate and conductance models respectively. Bath effects are included in the CT rate model through donor/acceptor population relaxation terms γ_D/γ_A and through pure dephasing terms γ_{mn} (not shown) of the system-bath Liouvillian (eqn. 4), which damp the coherences involving bridge states. Bath effects are included in the conductance model by coupling each bridge site to Buttiker probe electrodes (P=1… N) with couplings given by Γ_P.

The CT rate is computed from the reduced density matrix of a donor-bridge-acceptor system coupled to a bath, which is obtained by solving the quantum Liouville equation. In our simple model, the molecular bridge is connected to the donor (D) and acceptor (A). The donor with energy E_D is coupled to the first bridge site with interaction t_{D1}. An acceptor site (energy E_A) is connected to the Nth bridge site with coupling t_{NA}. The system Hamiltonian, $\hat{H}_S$, is:

$$\hat{H}_s = \hat{H}_{BR} + \sum_{m=D,A} |m > \varepsilon_m < m| + |D > t_{D1} < 1| + |1 > t_{D1} < D| + |A > t_{NA} < N| + |N > t_{NA} < A| \quad (2)$$

and the quantum Liouville equation is

$$\frac{d\rho}{dt} = -\frac{i}{\hbar}\hat{L}\rho = -\frac{i}{\hbar}(\hat{L}_S + \hat{L}_{SB})\rho \quad (3)$$

Here, the density matrix dynamics is determined by the Liouvillian $\hat{L} = \hat{L}_S + \hat{L}_{SB}$, which is a sum of the real system Liouvillian $\hat{L}_S = [\hat{H}_S, \rho]$ and the complex system-bath interaction Liouvillian, $\hat{L}_{SB}$, that accounts for the decay of the density matrix elements. Coupling of the D-B-A system electronic states to a bath introduces dissipative energy exchange between the system and the bath leading to population relaxation. Further, interaction with the bath creates a distribution of electronic transition energies leading to a decay of electronic coherences (dephasing). The bath is not described explicitly (through a microscopic model), and its influence on the system density matrix (population relaxation and dephasing) are included phenomenologically in the system-bath Liouvillian, $\hat{L}_{SB}$:

$$[\hat{L}_{SB}]_{mn,mn} = -i\left(\frac{\gamma_m}{2} + \frac{\gamma_n}{2} + \gamma_{mn}[1 - \delta_{mn}]\right) \quad (4)$$

Here, $\gamma_m/\hbar$ is the population relaxation rate from site m (inducing relaxation of the diagonal density matrix element ρ_{mm}), and $\gamma_{mn}/\hbar$ is the pure dephasing rate that accounts for coherence loss between sites m and n (ρ_{mn}). With this formulation, population relaxation on sites m and n (γ_m/γ_n) produces dephasing that causes coherences $\rho_{mn}(m \neq n)$ to decay, even if $\gamma_{mn}(m \neq n)$ is set to zero in eqn. 4. The time-dependent density matrix of eqn. 3 describes charge flow in the system.

At time t = 0, the charge is localized on the donor (ρ_{DD}=1 and all other diagonal/off-diagonal density matrix elements are zero). Eqn. 3 is then solved to determine the charge population on the acceptor as a function of time, $\rho_{AA}(t)$. This computation is accessible in the eigenstate basis

that diagonalizes the Liouvillian. Because the Liouvillian is complex, it has two sets of eigenvectors that connect the site basis to its eigenstates.[29, 30] The right (ket) eigenvectors X^R are defined by:

$$\hat{L}X^R = \varepsilon^R X^R \tag{5}$$

and the left (bra) eigenvectors X^L are defined by:

$$X^L\hat{L} = \varepsilon^L X^L \tag{6}$$

In practice, we compute the left eigenvector from $X^L = (X')^\dagger$ where X' is the eigenvector of $\hat{L}^\dagger$. Both left and right eigenvectors correspond to the same set of complex eigenvalues, $\varepsilon = \varepsilon^R = \varepsilon^L$, and are normalized as:

$$\tilde{X}^L = \frac{X^L}{\sqrt{X^L X^R}} \quad ; \quad \tilde{X}^R = \frac{X^R}{\sqrt{X^L X^R}} \tag{7}$$

These eigenvectors link the density matrix elements in the site basis to the density matrix elements in the eigenstate basis.

$$\rho_{mn}(t) = \sum_{a,b=1}^{N+2} \rho_{ab}(t)\, \tilde{X}^R_{mnab} \tag{8}$$

The pairs of indices *m,n* and *a,b* enumerate density matrix elements in the site basis (*m*, *n* = *D,A*, 1…*N*) and in the eigenstate basis (*a,b*=1…*N*+2), respectively. The time evolution of the density matrix elements in the site basis may be written in terms of the complex eigenvalues of the Liouvillian $\varepsilon_{ab} = [\hat{L}]_{abab}$:

$$\rho_{mn}(t) = \sum_{a,b,k,l=1}^{N+2} \rho_{kl}(0)\, \tilde{X}^L_{abkl}\tilde{X}^R_{mnab} e^{-\frac{i}{\hbar}\varepsilon_{ab}t} \tag{9}$$

The donor to acceptor CT rate constant k_{CT} is computed from the probability of charge (all on the donor site at time *t*=0) being transferred to the acceptor site at time *t*. Eqn. 10 defines the CT rate constant,k_{CT}, as the inverse of the average time, $<\tau_{AA}>$, to populate the acceptor; namely[31]

$$k_{CT} = \frac{1}{<\tau_{AA}>;} = \frac{\int_0^\infty \rho_{AA}(t)\,\mathrm{d}t}{\int_0^\infty t\rho_{AA}(t)\mathrm{d}t} \tag{10}$$

The rate in eqn. 10 is an activated rate, i.e charge transfer occurs when the donor and acceptor are resonant. Therefore, eqn. 10 does not include a description of nuclear relaxation following electron transfer. However, we now show that the rate constant k_{CT} in eqn. 10 is proportional to the non-adiabatic charge transfer rate constant k_{DA} between donor and acceptor

when the bridge is energetically well separated from the donor and acceptor.[32] For large energy separations between the donor and bridge states, the Hamiltonian in eqn. 2 may be transformed into an effective two-state Hamiltonian by a Löwdin partitioning scheme[33-35]:

$$\hat{H}_s = \sum_{i=D,A} |i> \varepsilon_i <i| + \ |D> t_{DA} <A| + |A> t_{DA} <D| \tag{11}$$

where t_{DA} is the effective electronic coupling between donor and acceptor. In the case of population relaxation only on the acceptor (i.e., γ_D =0) and $t_{DA} << \gamma_A$, eqn. 10 gives the analytical result $k_{CT} \sim 2|t_{DA}|^2 / \hbar\gamma_A$. Comparison of this result with the high-temperature non-adiabatic CT rate, given by

$$k_{DA} = \frac{2\pi}{\hbar}|t_{DA}|^2 \frac{1}{\sqrt{4\pi\lambda k_B T}} \ \exp\left(-\frac{(\Delta G^0+\lambda)^2}{4\lambda k_B T}\right) \tag{12}$$

where λ is the reorganization energy and ΔG^0 is the Gibbs free energy of reaction,[32] indicates that

$$k_{DA} = \frac{\pi\gamma_A}{\sqrt{4\pi\lambda k_B T}} \ k_{CT} \exp\left(-\frac{(\Delta G^0+\lambda)^2}{4\lambda k_B T}\right) \tag{13}$$

Thus, when the electronic states of the bridge are energetically distant from the donor/acceptor energies, the non-adiabatic charge transfer rate is given by k_{CT} in eqn. 10, evaluated for resonant donor-acceptor states and weighted by the Marcus activation factor. Both the prefactor and the Marcus activation factor in eqn. 13 depend only on properties of the donor/acceptor and are independent of the bridge (although λ and ΔG^0 are weakly distance dependent). Thus, the non-adiabatic charge transfer rate, k_{DA}, for donor-bridge-acceptor systems is linearly related to the rate constant k_{CT} that is defined by eqn. 10, when the donor and acceptor are the same.

Expression for the Electrochemical Rate Constant

In electrochemical experiments, the charge transfer occurs from an electrode surface to a molecular species (redox couple) such as ferrocene. The Gibbs free energy for the charge transfer reaction from an electrode state of energy ε is:

$$\Delta G^0 = \ \varepsilon_F - \varepsilon + e\eta \tag{14}$$

where η is the electrochemical overpotential and ε_F is the Fermi function of the electrode. In a density of states picture,[36] the electrochemical charge transfer rate from the donor electrode to the redox couple may be written by generalizing eqn. 13 as:

$$k_{EL} = \frac{\pi \gamma_A}{\sqrt{4\pi\lambda k_B T}} \int_0^\infty k_{CT}(\varepsilon) \exp\left(-\frac{(\varepsilon_F - \epsilon + e\eta + \lambda)^2}{4\lambda k_B T}\right) \rho_{EL} f_{EL}(\varepsilon) d\varepsilon \quad (15)$$

where ρ_{EL} is the density of states and $f_{EL}(\varepsilon) = [1 + \exp((\varepsilon - \varepsilon_F)/k_B T)]^{-1}$ is the Fermi distribution function. The standard heterogeneous rate constant is then given by the electrochemical rate at η=0

$$k^0 = \frac{\pi \gamma_A \rho_{EL}}{\sqrt{4\pi\lambda k_B T}} \int_0^\infty k_{CT}(\varepsilon) \exp\left(-\frac{(\varepsilon_F - \epsilon + \lambda)^2}{4\lambda k_B T}\right) f_{EL}(\varepsilon) d\varepsilon \quad (16)$$

In our rate calculations, we assumed T = 300 K, and λ = 0.8 eV, representative of the reorganization energy for the ferrocene redox couple that was used in the electrochemical measurements to determine the rates shown in Fig 1.[37]

Expression for the Molecular Conductance

The steady-state current in molecular conductance measurements is often modeled using a Landauer-Buttiker formulation in terms of non-equilibrium Green's functions.[38, 39] The conductance is modeled using the molecular bridge Hamiltonian of eqn. 1 with site 1 connected to a source electrode (L) and site N connected to a drain electrode (R). In addition, a Buttiker probe (P) electrode is located on each of the N bridge sites (see Fig. 2B). The Buttiker probe electrodes absorb current from the bridge sites and re-inject it into the bridge with a random phase. This 'scattered' current can travel to the acceptor electrode or to other Buttiker probe electrodes, and it can also be reflected back to the source through independent coherent channels. Thus, the Buttiker probes simulate phase breaking and backscattering events on the bridge. The bridge Green's function, including the influence of electrode contacts, is:

$$\boldsymbol{G}(E) = \frac{1}{(E\boldsymbol{I} - \boldsymbol{H}) - \boldsymbol{\Sigma}^L - \boldsymbol{\Sigma}^R - \sum_{P=1}^{N} \boldsymbol{\Sigma}_P} \quad (17)$$

Here, $\boldsymbol{H}$ is the molecular bridge Hamiltonian of eqn. 1, and $\boldsymbol{I}$ is the identity matrix. The influence of electrodes L and R and of the Buttiker probes on the bridge are included in the bridge Green's function through the complex self-energy matrices $\boldsymbol{\Sigma}^L$, $\boldsymbol{\Sigma}^R$, and $\boldsymbol{\Sigma}_P$, respectively. The real (imaginary) parts of the self-energy matrix elements add to the corresponding elements of the bridge Hamiltonian and manifest themselves through shifts (broadenings) of the molecular orbital energies in the local density of states (LDOS):[38, 39]

$$LDOS(E) = \frac{i}{2\pi} Tr[\boldsymbol{G}(E) - \boldsymbol{G}^{\dagger}(E)\,] \tag{18}$$

where $\boldsymbol{G}^{\dagger}$ is the Hermitian adjoint of $\boldsymbol{G}$. Applying a potential bias across electrodes L and R causes a current to flow between the electrodes. This current $I(L \to R)$ is

$$I(L \to R) = \frac{2e}{h} \int \left[T_{LR}(E)[f_L(E) - f_R(E)] + \sum_{P=1}^{N} T_{PR}(E)[f_P(E) - f_R(E)] \right] dE \tag{19}$$

where $T(E)$ is the transmission function and $f(E)$ is the Fermi function. $T(E)$ between a pair of electrodes m and n (m,n=L,R,P) is

$$T_{mn}(E) = Tr[\boldsymbol{\Gamma}^{m} \boldsymbol{G} \boldsymbol{\Gamma}^{n} \boldsymbol{G}^{\dagger}] \tag{20}$$

The $\boldsymbol{\Gamma}$ (broadening) matrices for each electrode m are defined as: $\boldsymbol{\Gamma}^{m}$ = [$\boldsymbol{\Sigma}^{m}$ - ($\boldsymbol{\Sigma}^{m}$)†]. The Fermi functions $f_m(E)$ describe the electron occupancy of the states in the m=L, R, P electrodes at energy E:

$$f_m(E) = [1 + \exp((E - \mu_m)/k_B T)]^{-1} \tag{21}$$

The Fermi functions for the source (L) and drain (R) electrodes are defined by their chemical potentials: $\mu_L = E_F - eV/2$ and $\mu_R = E_F + eV/2$. Here, E_F (the Fermi energy of the electrodes) and V (the potential bias) are parameters. The chemical potential μ_P of a Buttiker probe at site P is unknown, but it can be determined from the constraint on each Buttiker probe P to absorb no net current:[40]

$$I_P = 0 = \frac{2e}{h} \int \left[T_{LP}(E)[f_L(E) - f_P(E)] + T_{RP}(E)[f_R(E) - f_P(E)] \right.$$
$$\left. + \sum_{\substack{P'=1 \\ P' \neq P}}^{N} T_{P'P}(E)[f_{P'}(E) - f_P(E)] \right] dE \tag{22}$$

By making the further simplifying assumption that the net current absorbed by each Buttiker probe at energy E is zero, the integrand in eqn. 22 may be set to zero for each probe. This condition means that the scattering by each probe is elastic. The unknown Fermi functions f_P are obtained by solving the resulting N coupled differential equations on a discrete energy grid. In the Landauer-Buttiker approach described here, charges are exchanged with the system only at electrodes L and R. The Buttiker probe electrodes are elastic scattering centers for resonant

current. Scattering of the current at the Buttiker probes leads to phase relaxation of the carriers without any momentum or energy relaxation.

In our numerical simulations, the steady-state current between electrodes was calculated using eqns. 19 through 22 for a potential bias V=0.1 V and T=300 K. In this model, both thermally activated, and tunneling currents can be computed, including bath-induced decoherence. However, inelastic current contributions arising from interactions of the charge with molecular vibrational modes [41-43] are not considered within the approximations of the model. The conductance (σ) is calculated as:

$$\sigma = I(\mathrm{L}\rightarrow\mathrm{R})/V \tag{13}$$

We end this section with a discussion of how population relaxation and decoherence effects are incorporated in the rate and conductance models, and of the assumptions that we make to enable a comparison of charge transport among the models. Both rate and conductance models include bath-induced relaxation of diagonal (populations) and off-diagonal (coherences) elements of the system density matrix. In the rate model, the bridge is coupled to the donor and acceptor (Fig 2A) that are, in turn, connected to the bath continuum through the lifetime parameters γ_D and γ_A. As given by eqn. 4, these lifetime contributions (imaginary terms in the diagonal elements of the Hamiltonian) also contribute to the relaxation of coherences between bridge and donor/acceptor states. In the conductance model, the bridge is directly coupled (at sites 1 and N in Fig 2B) to a continuum of electrode states through the broadening matrices Γ_L and Γ_R. Analogous to the rate model, the broadening matrices add imaginary terms to the diagonal elements of the Hamiltonian (see eqn. 17) and hence contribute towards both population as well as coherence relaxation. Further, in the conductance model, the Buttiker probe couplings Γ_P also add imaginary terms to the Hamiltonian which might appear to be equivalent to adding lifetime broadening terms to the bridge ($\gamma_{m,}$, where m=bridge sites) in the CT rate model. However, there is a critical difference. In the conductance model, the conductance is computed with zero current absorption at each Buttiker probe. This is equivalent to eliminating the population relaxation contributions provided by Γ_P, while retaining its dephasing contributions. On the other hand, adding lifetime broadening couplings (γ_m) to the bridge in the CT rate model leads to irreversible population relaxation from the bridge. To avoid population loss from the bridge to the bath, we set all lifetime broadening terms $\gamma_{m,}$= 0 (m = bridge sites) in the rate

model. We then control the decoherence in the CT rate model through the pure dephasing term γ_{mn} of the system bath Liouvillian (see eqn. 4) which does not have an analog in the conductance model. Thus, while the decoherence in the conductance model arises from lifetime broadening (Γ_P) of bridge-state energies (see eqn. 17) because of its coupling to Buttiker probes (a variable parameter in our calculations), the decoherence in the CT rate model arises from lifetime broadening of the donor and acceptor state energies (fixed for a given donor-acceptor pair) and through γ_{mn} (variable parameter in our calculations). While this approach allows comparison of the decoherence effects in the CT rate and conductance models on a similar footing, it is based on phenomenological descriptions of decoherence in the rate and the conductance models which are not entirely equivalent. The extent of decoherence in the rate and conductance models can thus only be compared qualitatively, e.g., how the decoherence influences the distance dependence of CT in the two models. In our numerical simulations, we demonstrate that using different models to describe rates and conductance does not limit our conclusions regarding the influence of dephasing rates and CT energy barriers on the rate-conductance correlation.

Numerical Results and Discussion

The theoretical framework developed above is now used to calculate the CT rate and the molecular conductance as a function of the bridge length *N*. The change in CT rate and molecular conductance as a function of bridge length provides information on the underlying charge-transport mechanism. When the donor is energetically well separated from the bridge, charge transport occurs predominantly via superexchange for short bridge lengths, and the molecular conductance or CT rate drops approximately exponentially with the bridge length. Beyond a certain bridge length, determined by the donor-bridge energy gap and the temperature, thermal activation of the charge to populate bridge states becomes competitive with tunneling, and the distance dependence softens -- approaching an ohmic ($1/N$) dependence for long bridges. Previous theoretical analysis[29, 44] has found that the transition to a $1/N$ distance dependence is gradual, and that the fall off in CT rate may even appear distance independent, for intermediate bridge lengths.

1. Distance Dependence of Charge Transport with Decoherence

Fig. 3 compares the calculated distance dependence for the CT rate and the molecular conductance in a model system with identical CT energy barriers, $E_{DB} = E_{FB}$, but with variable bath-induced decoherence. The CT rates and conductances show an exponential distance dependence at short bridge lengths with a crossover to a softer distance dependence at longer bridge lengths. Interestingly, the distance dependences of the CT rate and the molecular conductances are not identical (note that in Fig. 3A both rates and conductance are normalized with respect to their values at 1 BU which allows us to compare their distance dependence). The

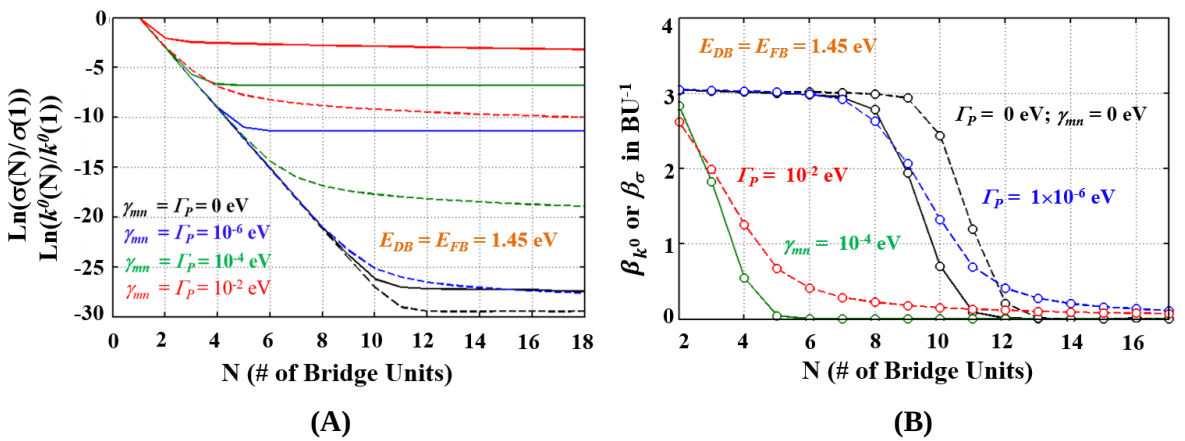

(A) **(B)**

Figure 3: (A) This plot shows the distance dependence of the electrochemical rate constant (solid line) and molecular conductance (dashed lines) normalized with respect to their values at 1 BU. Rate constants were calculated using eqn. 10 (E_{DB} = 1.45 eV; V_{BB}= 0.3 eV; V_{D1}= 0.1 eV; V_{NA}= 0.1 eV; γ_D = 1×10^{-16} eV; γ_A = 0.1 eV; γ_m = 0 eV m=bridge sites). Molecular conductances were calculated using eqn. 13 (E_{FB} = 1.45 eV; V_{BB} =0.3 eV; Γ_{L1}= 0.1 eV; Γ_{NR} = 0.1 eV). The model system parameters for the bridge most closely resemble alkanethiol chains, however the CT energy gap and dephasing parameters were chosen to facilitate the discussion and may not reflect values present in actual experiments. The colored lines show the effect of pure dephasing (included by varying γ_{mn} and Γ_P) on the distance dependence of the CT rate/molecular conductance. To minimize the number of parameters only γ_{mn} terms controlling the decay of coherences between donor/acceptor and bridge states were set to the values shown in the figure (i.e γ_{DA} = 0, γ_{mn} =0 when both m and n are bridge sites; trial calculations showed that non-zero values of these terms do not alter the general trends in distance dependence of rates considered here or our final conclusions). (B) The distance decay constants β_{k^0} for CT rates (solid lines) and β_σ for molecular conductance (dashed lines) are plotted versus the number of bridge units for the different dephasing rates. The β values for bridge unit N was calculated by fitting the N dependence of $\ln(k^0)$ or $\ln(\sigma)$ for three values from N-1 to N+1.

distance dependence of CT rate and conductance coincide only at short bridge lengths with deviations appearing near the crossover region from exponential to soft distance dependence. Because thermally-activated transport competes with tunneling transport near the cross-over region, the differences in distance dependence of the CT rates and conductances are associated with model parameters that control resonant CT processes. Specifically, the difference occurs

because of differences in the treatment of bath-induced decoherence in the rate and conductance models.

In the conductance analysis, dephasing contributions arise from the coupling (Γ_P) of the bridge to the Buttiker probes (imaginary part of the self-energy Σ_P in eqn. 17). For CT, dephasing is introduced via two parameters in the system bath Liouvillian (eqn. 4): (1) the population relaxation terms (γ_m) and (2) the pure dephasing γ_{mn} ($m \neq n$) terms. This feature results in CT rate models that contain non-zero dephasing contributions from the donor/acceptor population relaxation ($\gamma_{D/A}$), even after zeroing the γ_{mn} and γ_m ($m \neq$ D, A) contributions for the bridge states. In contrast, the conductance model with $\Gamma_P = 0$ includes no dephasing contributions and leads to a distance dependence of conductance which differs from that of the CT rates. The conductance computed for a Buttiker probe coupling value of 10^{-6} eV (dashed blue line) produces a distance dependence that closely matches the computed CT rate with $\gamma_{mn} = 0$ (solid black line). Because the bridge parameters and the CT energy gaps are constrained to be the same for rate/conductance calculations, we infer qualitatively that dephasing(k^0) ~ dephasing(σ) for the rate model with $\gamma_{mn} = 0$ (solid black line) and the conductance model with $\Gamma_P = 10^{-6}$ eV (dashed blue line). This qualitative comparison between different phenomenological models for incorporating bath-induced decoherence in the CT rate and conductance is justified because both models of decoherence produce the same effect on the distance dependence of CT transport (see Fig. 3A and discussion below).

Earlier studies[26,6] found that bridge decoherence can significantly influence the distance dependence of CT rates/molecular conductances. Fig. 3 shows that, for large CT energy barriers, dephasing changes the distance dependence of both the CT rate and the molecular conductance in similar ways. For both rates and conductances, the crossover from an exponential distance dependence to a nearly distance-independent regime shifts to shorter bridge lengths for larger bridge decoherence (larger values of γ_{mn} and Γ_P). Bath-induced decoherence broadens the bridge state energies, effectively reducing the tunneling barrier and boosting both the superexchange and thermally activated transport rates.[45] Decoherence also introduces backscattering, which reduces ballistic (activated but coherent) CT.[45] Fig. 3A shows that increasing the decoherence makes the thermally activated transport mechanisms more competitive with the superexchange for shorter bridges, leading to the observed shift in the crossover region.

To draw a link between the data in Fig. 3A and the experimental observations in Fig. 1, we fit a decay length β to the distance dependence of rates/conductances. In experiments, β_σ and β_{k^0} are often extracted from linear fits to experimentally measured $\ln(k^0/s^{-1})$ or $\ln(\sigma/\Omega^{-1})$ (typically 3-10 BU).[10, 11, 19, 20] Accordingly, β_σ and β_{k^0} values were calculated as a function of the number of bridge units (N) by linearly fitting three data points for $\ln(k^0/s^{-1})$ or $\ln(\sigma/\Omega^{-1})$ computed for N-1, N, and N+1 bridge units. The variation in β_σ and β_{k^0} as a function of N and with different levels of bath induced decoherence is shown in Fig. 3B. With increasing bridge length, both β_σ and β_{k^0} switch over from a value of 3 BU^{-1} to ~ 0 BU^{-1} signifying a change from superexchange to hopping CT. The increase in dephasing contributions tends to lower both β_σ and β_{k^0} at all bridge lengths (compare red dashed line with black dashed line or green solid line with black solid line), although at intermediate dephasing values the effects are more complex and exhibit a bridge length dependence (compare blue dashed line with black dashed line). Notably, the ratio β_σ/β_{k^0} which dictates the power law in Fig. 1, approaches unity only when the dephasing(k^0) ~ dephasing(σ).

To summarize, Fig. 3 indicates that bath-induced decoherence can significantly change the distance dependence of both the CT rate and the molecular conductance, even if the electronic structure of the bridge is only weakly perturbed. Thus, different distance dependences could be produced by experiments that measure molecular conductances (e.g., STM-BJ) and CT rates (e.g., measured with electrochemistry) for identical molecular bridges, because of different medium interactions. While the crossover from an exponential to a soft distance dependence has been observed in experiments for a number of CT rate studies, the molecular conductance measurements for the same set of molecules are often exponential within the same bridge-length range, exhibiting no crossover.

2. Distance Dependence of Charge Transport with Varying CT Energy Barriers

We now explore how the magnitude of the CT energy barriers (parameters E_{DB} and E_{FB}, from Fig. 2) influence β_σ and β_k. For superexchange, β should decrease as the barrier decreases;[34, 46-48,9] and the crossover point from exponential to 1/*N* behavior should shift to shorter chain lengths for lower barriers.[49] The distance dependence of the CT rate and the molecular conductance were calculated for: 1) E_{DB}= E_{FB}=1.45 eV, 2) E_{DB}= E_{FB}=1.15 eV, and 3) E_{DB}= E_{FB}=0.75 eV. The

values of the parameters Γ_p and γ_{mn} were chosen such that dephasing(k^0) ~ dephasing(σ) based on the comparison of distance dependence of rates and conductances at E_{DB}= E_{FB}=1.45 eV. Fig. 4A

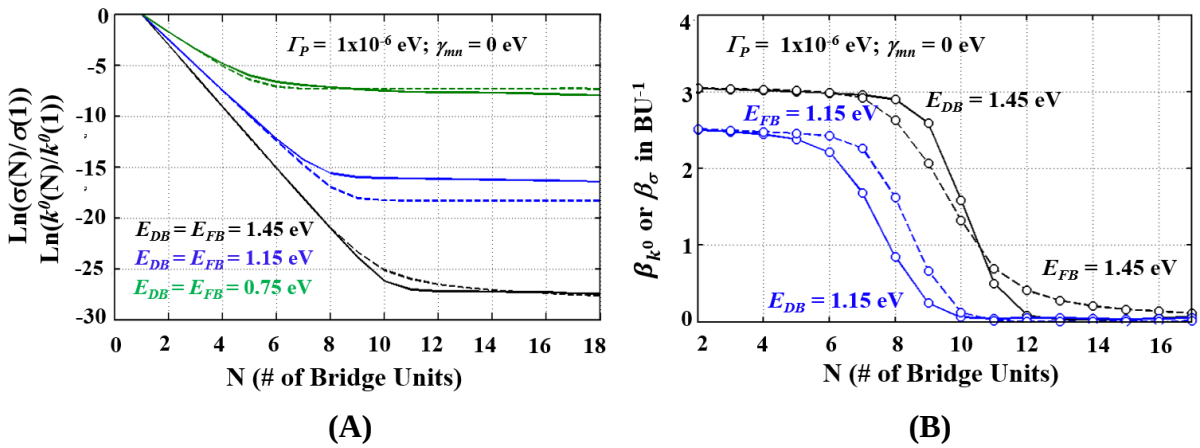

Figure 4: (A) Dependence of CT rates (solid lines) and molecular conductance (dashed lines) on bridge length for different energy barrier heights (colored lines) and dephasing(k^0) ~ dephasing(σ) in the rate/conductance models. Rate/conductance values are normalized with respect to their values at 1 BU (B) Variation of the distance decay constants β_{k^0} for CT rates (solid lines) and β_σ for molecular conductance (dashed lines) with the number of bridge units. The calculations were performed for two different values of the CT barriers; all other parameters are the same as the model system described in Fig. 3.

shows that for this minimal dephasing model (γ_{mn} =0 eV; Γ_P =10^{-6} eV), decreasing the CT energy barrier shifts the crossover region (from an exponential to a soft distance dependence) to shorter bridge lengths for both CT and molecular conductance. Decreasing the barrier also decreases β (Fig. 4B) and is attributed to: (1) an increase in tunneling probability and (2) an increase in the probability of thermally activated CT. The slight dip in the conductance curves (dashed green) around 6 BU in Fig. 4A is not a crossover point (from exponential to soft distance dependence); rather the CT energy barrier (E_{FB}=0.75 eV) is small enough that the conductance has thermally-activated contributions for all bridge lengths (showing soft distance dependence). In summary, the relative values of β_σ and β_{k^0} are significantly modulated by the CT energy barrier in conductance and rate measurements. The data in Fig. 4B show that $\beta_\sigma \neq \beta_{k^0}$ when $E_{DB} \neq E_{FB}$ (compare β values given by the solid and dashed lines of different colors). Thus, E_{DB}= E_{FB} (compare β values given by the solid and dashed lines of the same color) is a necessary condition (along with dephasing(k^0) ~ dephasing(σ)) for the power law exponent β_σ/β_{k^0} in Fig. 1 to be unity.

3. Relationship between Molecular Conductance and the Electrochemical Rate Constant

The results in the previous sections (Figs. 3B and 4B) indicate that the CT energy barrier and bath induced decoherence strongly influence the distance dependence of rates and conductances. Previous theoretical studies for high barriers[1, 2] found that the CT rates in both the superexchange and the hopping regimes are proportional to the conductances. In contrast, experiments (Fig. 1)

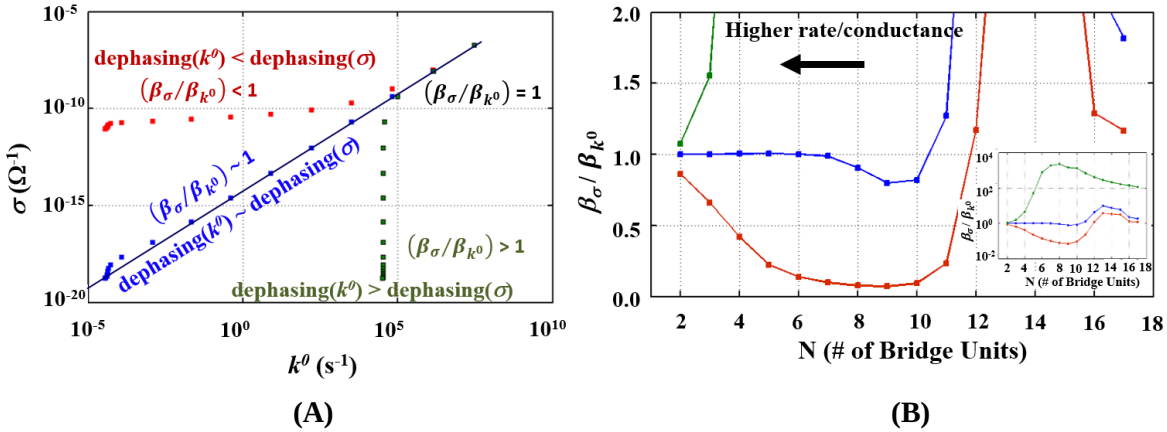

(A) **(B)**

Figure 5: (A) Correlation between the CT rate and the molecular conductance for the three cases of relative dephasing rates on the bridge. The black line indicates a linear correlation between conductance and rate: σ=A×$(k^0)^m$ (where m= β_σ/β_{k^0}=1). (B) The exponent m= β_σ/β_{k^0} calculated for the data in panel (A) as a function of bridge length. Red blue and green lines/symbols correspond to the exponents obtained from fits to the red blue and green symbols in panel (A) respectively. Inset shows the full range of exponents on a logscale (β_σ/β_{k^0} for the green line reaches very large values as β_{k^0} ~ 0) obtained at all bridge lengths. Data in panel (B) is restricted to exponent values between 0-2 and shows that m=1 is obtained over a large range of rates/conductances only when the dephasing rates in the rate and conductance models are similar. The rate-conductance is non-linear (m ≠ 1) over the whole data range, when the dephasing rates in the rate and conductance models are different.

find that the rate-conductance relationship follows a power law:[20]

$$\sigma = \sigma_{(L=0)} \times \left(\frac{k^0}{k^0_{(L=0)}}\right)^{(\beta_\sigma/\beta_{k^0})} \qquad (14)$$

Because the observables are measured under different experimental conditions, the bridge decoherence and the CT energy barriers are likely to be different, leading to $\beta_\sigma \neq \beta_{k^0}$.

Fig. 5 shows how decoherence rate differences between the measurements influence the correlation between σ and k_{CT} (for the data from Fig. 4A). We consider three cases of relative decoherence (as determined from the distance dependence data in Fig. 4A) in rate and conductance models: 1) dephasing(k^0) < dephasing(σ) (red symbols; γ_{mn} =0 eV; Γ_P =10^{-2} eV), 2) dephasing(k^0) ~ dephasing(σ) (blue symbols; γ_{mn} =0 eV; Γ_P =10^{-6} eV), and 3) dephasing(k^0) >

dephasing(σ) (green symbols; γ_{mn} =10^{-4} eV; Γ_P =10^{-6} eV) where the CT energy barriers in the CT rate and the molecular conductance models are the same (E_{DB} = E_{FB} = 1.45 eV). The correlation between rates and conductance is plotted on a log-log scale, so that the slope of the correlation is the ratio β_σ/β_{k^0}. The black line represents a linear correlation (unit slope) between rate and conductance. The rate constant and the conductance are only linearly correlated for bridge lengths where their distance dependence is identical, i.e. $\beta_\sigma = \beta_{k^0}$. Fig. 5 shows that for fixed barrier heights, the correlation is linear (m= β_σ/β_{k^0}=1) over a large range (over 10 orders of magnitude) of conductances and rates when dephasing(k^0) ~ dephasing(σ) (blue symbols in Fig. 5). Deviation from linearity occurs near the crossover point (above 8 BU in fig 5 B) from exponential to soft distance dependence. Because the dephasing rates in the two models are similar but not identical, the distance dependence for rates and conductances near the cross-over point differs (compare solid black and dashed blue lines in Fig. 4) leading to non-linearity in the rate-conductance relation at long bridge lengths. In contrast, when the dephasing rates in the two models differ significantly, the non-linearity in the rate-conductance relation is evident over the entire range of data at all bridge lengths. When dephasing(k^0) < dephasing(σ) (red symbols in Fig. 5), the crossover from exponential to soft distance decay occurs much earlier for the conductance (compare solid black and dashed red lines in Fig. 4). As a result, the rate conductance correlation is close to linear only at short bridge lengths where superexchange CT dominates. Fig 5B shows m≠1 even for rates/conductances across 1 BU. At longer bridge lengths, β_σ drops much more rapidly than β_{k^0} because of stronger dephasing in the conductance model to give a ratio β_σ/β_{k^0} < 1. A complementary decoupling of the rate and conductance is evident in the other limit: dephasing(k^0) > dephasing(σ) (dark green symbols in Fig. 5) where the crossover from an exponential to a softer distance decay occurs earlier for the rates (compare solid green and dashed blue lines in Fig 4). As before, a near-linear correlation appears for short bridges where superexchange CT dominates. For longer bridges, β_{k^0} drops much faster than β_σ because of stronger dephasing in the rate model to give a ratio β_σ/β_{k^0} > 1. This analysis suggests that the power law exponent (m=β_σ/β_{k^0} ~ 0.6 – 0.9 < 1) obtained from fits to the experimental rate versus conductance data in Fig. 1 may arise from larger dephasing rates in conductance measurements than in the rate measurements (see red symbols in Fig 5B). Note that the numerical values of β_σ/β_{k^0} from Fig 5B were obtained for a model system (caption of Fig 3).

Thus, while the analysis in Fig 5 provides general insights to understand the trends in the rate-conductance scaling exponents (β_σ/β_{k^0}) as a function of dephasing, the numerical values in Fig 5B do not correspond to exponents of the experimental data in Fig 1. The extent to which dephasing influences the non-linearity shown in Fig 1 can be determined only through quantitative fits of the framework developed here to the experimental data, a task which we will undertake in a separate study. An important point is that the decay constants (β_σ and β_{k^0}) for pure superexchange transport are not influenced by changes in the dephasing rates (slopes of the

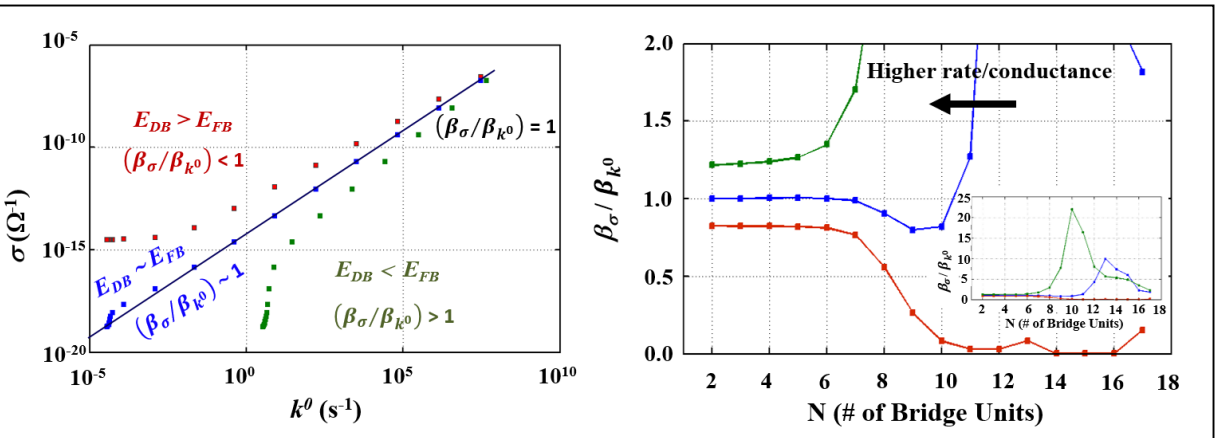

Figure 6: (A) Correlation between the CT rate and the molecular conductance for three different CT energy barrier conditions: (i) E_{DB} (1.45 eV) > E_{FB} (1.15 eV), E_{DB}=E_{FB} (1.45 eV), and (iii) E_{DB} (1.15 eV) < E_{FB} (1.45 eV). The black line indicates a linear correlation (m = β_σ/β_{k^0}=1). (B) The exponent m= β_σ/β_{k^0} calculated for the data in panel (A) as a function of bridge length. Red blue and green lines/symbols correspond to the exponents obtained from fits to the red blue and green symbols in panel (A) respectively. Inset shows full range of exponents obtained at all bridge lengths. Data in panel (B) is restricted to exponent values between 0-2 and shows that m=1 is obtained over a large range of rates/conductances only when the energy barriers in the rate and conductance models are same. The rate-conductance is non-linear (m ≠ 1) over the whole data range, when the energy barriers in the rate and conductance models are different.

exponential decay of rates/conductances with bridge length in Fig 3 do not change with dephasing rates). This means that it is possible to find linear correlations (m=β_σ/β_{k^0} ~ 1) between rates and conductances at short bridge lengths, despite the significant differences in dephasing rates in the two models. The near linear correlation at short bridge lengths in Fig 5A is a manifestation of this effect.

The magnitude of the CT barrier also affects the correlation between the CT rate and the molecular conductance. Fig. 6 shows a log-log plot of the rate-conductance correlation (as in Fig. 5), but for the three cases of relative CT energy barriers (see Fig. 6 caption) in the rate and the conductance models. Both models have similar dephasing rates (γ_{mn} = 0 eV; Γ_P = 10^{-6} eV) as in

case 2 of Fig. 5. The rate-conductance correlation for $E_{DB} = E_{FB}$ (blue symbols in Fig. 6) is the same as case 2 of Fig. 5, indicating a near linear correlation for a wide range of bridge lengths. As discussed above, the non-linearity for long bridge lengths arises because the dephasing in the rate and conductance models are not identical. In contrast, when the CT energy barriers in the two models are different, the rate-conductance correlation is non-linear at all bridge lengths. When $E_{DB} > E_{FB}$ (red symbols), the superexchange CT rate drops more rapidly and the crossover of the rate to a softer distance dependence occurs at longer bridge lengths than for the conductance. Consequently, β_{k^0} is larger than $\beta_{\sigma,}$ and $\beta_{\sigma}/\beta_{k^0} < 1$ for all bridge lengths. The situation is reversed when $E_{DB} < E_{FB}$ (green symbols), as the conductance drops more rapidly than the rate in the superexchange regime with crossover to a weaker distance dependence occurring at longer bridge lengths than that for the rate. Consequently, β_{σ} is larger than β_{k^0} and the ratio $\beta_{\sigma}/\beta_{k^0} > 1$ for all bridge lengths. This analysis on our model system (parameters given in caption of Fig 3B) indicates that the exponent in the power law fits ($\beta_{\sigma}/\beta_{k^0}$ ~0.6 - 0.9 < 1) of Fig. 1 may arise from smaller CT barriers in the conductance measurements than in the rate measurements (red symbols in Fig 6B). Note that decay constants (β_{σ} and β_{k^0}) for pure superexchange transport are strongly dependent on the energy barriers for charge transport (slopes of the exponential decays of rates/conductances with distance in Fig 4A change with the CT energy barrier). Thus, when energy barriers for charge transport are significantly different, the rate/conductance correlation can never be linear (m=$\beta_{\sigma}/\beta_{k^0} \neq 1$) as seen in Fig 6A and 6B.

4. General role for dephasing and CT energy barriers in shaping the non-linear relationship between charge transport measurements

In this section, we show that our findings regarding the origin of the rate-conductance non-linearity are in fact generally applicable to the study of correlations between any two charge transport measures (rates or conductances). In other words, the same property (for example, two CT rates or two conductances) when measured subject to conditions where the environmental decoherence contributions and/or CT energy barriers are different, will exhibit a non-linear correlation. Fig. 7 shows the correlation between two CT rates ($k^0$1 and $k^0$2 in Fig 7A) and two conductances (σ1 and σ2 in Fig 7B) computed for identical charge transfer barriers (E_{DB} ($k^0$1) = E_{DB} ($k^0$2) and E_{FB} (σ1) = E_{FB} (σ2)), but with three choices of the relative dephasing rates (γ_{mn}

($k^0$1) < γ_{mn} ($k^0$2), γ_{mn} ($k^0$1) = γ_{mn} ($k^0$2), γ_{mn} ($k^0$1) < γ_{mn} ($k^0$2) and Γ_P (σ1) < Γ_P (σ2), Γ_P (σ1) < Γ_P (σ2), Γ_P (σ1) < Γ_P (σ2)). The data in Fig 7 can be directly compared with that in Fig 5 and show a non-linear rate-rate and conductance-conductance correlation dependent on the relative dephasing rates, similar to the behavior exhibited by the rate-conductance correlation. The non-linear rate-conductance trends seen in Fig 1 may also be seen for two series of CT rate measurements (or two conductance measurements) when environment-induced decoherence contributions in the two experimental setups are different. The calculations shown in Fig 7 also help validate the robustness of our conclusions on how dephasing influences the rate-conductance correlation. The trends in the rate-conductance correlation shown in Fig 5 were obtained by comparing two different model calculations (the CT rate model based on the reduced density matrix framework and the conductance model based on the Landauer-Buttiker framework). A concern arises that the non-linear rate-conductance correlation obtained in Fig 5 may arise from differences in model assumptions and parameters. For instance, there is no

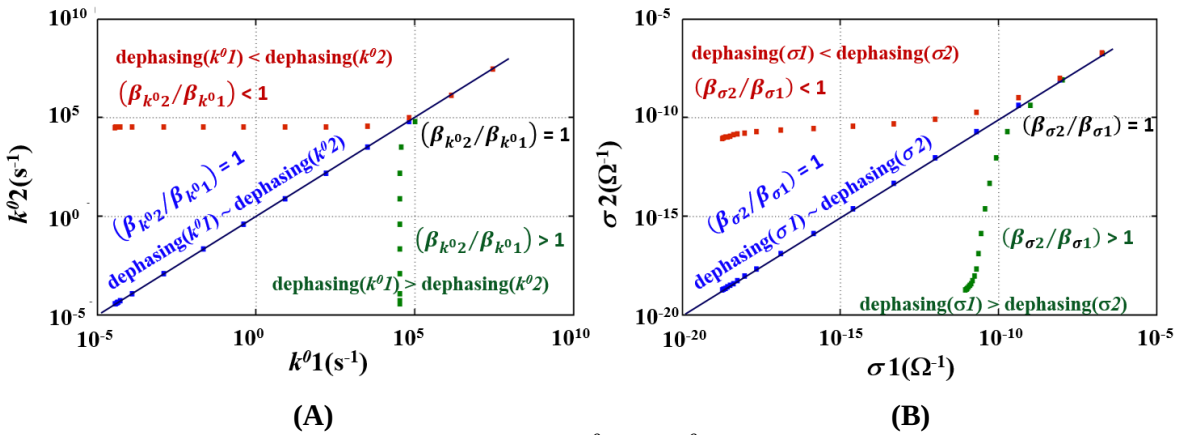

Figure 7: (A) Correlation between two CT rates $k^0$1 and $k^0$2 computed as a function of bridge length with identical CT energy barriers (E_{DB} ($k^0$1) = E_{DB} ($k^0$2) = 1.45 eV)) but for three different conditions of relative dephasing: (i) γ_{mn} ($k^0$1) = 0 eV < γ_{mn} ($k^0$2)= 10^{-4} eV, (ii) γ_{mn} ($k^0$1) = 0 eV = γ_{mn} ($k^0$2) and (iii) γ_{mn} ($k^0$1) = 10^{-4} eV > γ_{mn} ($k^0$2)= 0 eV. (B) Correlation between two conductances σ1 and σ2 computed as a function of bridge length with identical CT energy barriers (E_{FB} (σ1) = E_{FB} (σ2) = 1.45 eV)) but for three different conditions of relative dephasing: (i) Γ_P (σ1) = 10^{-6} eV < Γ_P (σ2)= 10^{-2} eV, (ii) Γ_P (σ1) = 10^{-6} eV = Γ_P (σ2) and (iii) Γ_P (σ1) = 10^{-2} eV > Γ_P (σ2)= 10^{-6} eV. The black lines in both panels indicate a linear correlation (m = β_{k^0}1 /β_{k^0}2=1) in (A) and (m = $\beta_{\sigma 1}$ /$\beta_{\sigma 2}$=1) in (B).

theoretical expression to directly link the numerical values of dephasing in the CT rate models to those of the conductance models (see discussion following eqn. 13 in the "Theoretical Models" section). The strong agreement among the trends in the data of Fig 7, where comparisons are within the same model framework (between CT rate models or between conductance models),

and the data of Fig 5, justifies our assumptions for comparing dephasing rates between rate and

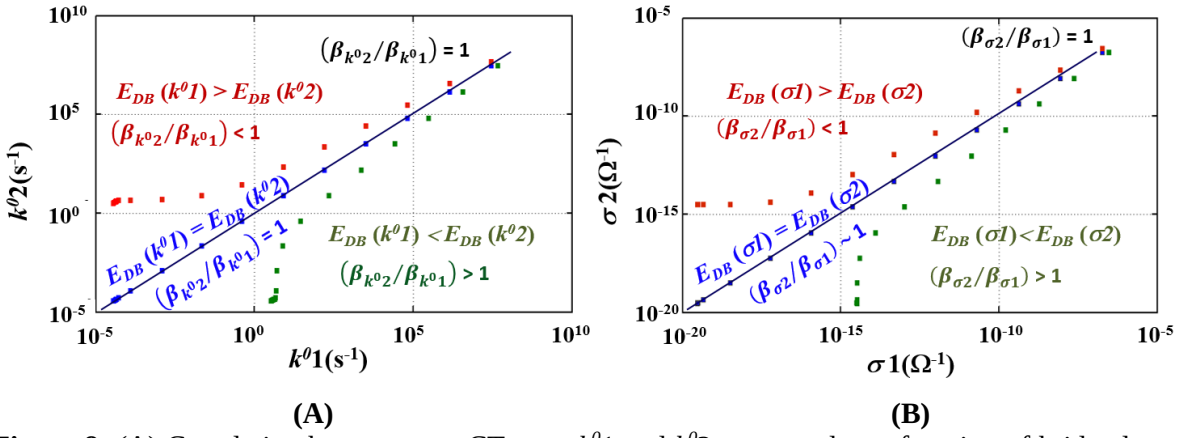

(A) **(B)**

Figure 8: (A) Correlation between two CT rates $k^0 1$ and $k^0 2$ computed as a function of bridge length with identical dephasing rates (γ_{mn} ($k^0 1$) = 0 eV = γ_{mn} ($k^0 2$)) but for three different conditions of relative CT energy barriers: (i) E_{DB} ($k^0 1$) = 1.15 eV < E_{DB} ($k^0 2$) = 1.45 eV, (ii) E_{DB} ($k^0 1$) = E_{DB} ($k^0 2$) = 1.45 eV and (iii) E_{DB} ($k^0 1$) = 1.45 eV > E_{DB} ($k^0 2$) = 1.15 eV. (B) Correlation between two conductances $\sigma 1$ and $\sigma 2$ computed as a function of bridge length with identical dephasing rates (Γ_P ($\sigma 1$) = 10^{-6} eV = Γ_P ($\sigma 2$)) but for three different conditions of relative CT energy barriers: (i) E_{FB} ($\sigma 1$) = 1.15 eV < E_{FB} ($\sigma 2$)= 1.45 eV, (ii) E_{FB} ($\sigma 1$) = 1.45 eV = E_{FB} ($\sigma 2$) and (iii) E_{FB} ($\sigma 1$) = 1.45 eV > E_{FB} ($\sigma 2$) = 1.15 eV. The black lines in both panels indicate a linear correlation (m = $\beta_{k^0} 1 / \beta_{k^0} 2$=1) in (A) and (m = $\beta_{\sigma 1} / \beta_{\sigma 2}$=1) in (B).

conductance models to extract the factors behind the rate-conductance non-linearity.

Our conclusions regarding the influence of the CT energy barrier on the rate-conductance correlation can also be extended to rate-rate and conductance-conductance correlations. Fig. 8 shows the correlation between two CT rates ($k^0 1$ and $k^0 2$ in Fig 8A) and two conductances ($\sigma 1$ and $\sigma 2$ in Fig 8B) computed for identical dephasing rates (γ_{mn} ($k^0 1$) = γ_{mn} ($k^0 2$) and Γ_P ($\sigma 1$) = Γ_P ($\sigma 2$)) but with three cases of relative CT energy barriers (E_{DB} ($k^0 1$) < E_{DB} ($k^0 2$), E_{DB} ($k^0 1$) = E_{DB} ($k^0 2$), E_{DB} ($k^0 1$) > E_{DB} ($k^0 2$) and E_{FB} ($\sigma 1$) < E_{FB} ($\sigma 2$), E_{FB} ($\sigma 1$) = E_{FB} ($\sigma 2$), E_{FB} ($\sigma 1$) > E_{FB} ($\sigma 2$)). The data in Fig 8 show that the rate-rate and conductance-conductance correlations are non-linear, influenced by relative CT energy barriers similar to that seen for the rate-conductance correlation in Fig 6. Thus, the non-linear rate-conductance trends observed in Fig 1 are also observed for two series of CT rate measurements (or two conductance measurements) when the CT energy barriers in the two experimental setups are different (e.g., obtained using different electrode binding linkers/redox reporters molecular designs or different electrode materials).

Conclusions

The analysis in this paper indicates that the CT energy barrier and decoherence on the bridge can independently, or in combination, influence the predicted rate-conductance relationship, producing a non-linearity in the power law seen in Fig. 1. Specifically, our numerical simulations show that the scaling exponent ($m=\beta_\sigma/\beta_{k^0} \sim 0.6 – 0.9 < 1$) in the rate-conductance correlation of Fig 1, may arise under conditions where dephasing (conductance) > dephasing (rate) and/or from $E_{DB} > E_{FB}$. Replacing a molecular donor/acceptor with an electrode introduces a continuum of electrode states, which provides an additional source of broadening for the bridge states. Because an electrode provides irreversible decay channels for charge population on the bridge, population relaxation and dephasing rates on the bridge are expected to be greater when coupled to electrodes rather than to molecular donors and acceptors. Overall, decoherence effects are expected to increase with the number of electrodes connected to the bridge. Thus, we expect decoherence (D-B-A) < decoherence (M-B-A/D-B-M) < decoherence (M-B-M). However, other medium effects may vary among experimental schemes as well. Molecular bridges coupled to electrodes will experience stabilization of electronic states from electrode polarization in response to injection of charge on the bridge.[50, 51] Image charge effects of this kind can lead to modified charge transfer barriers in the different experiments, even when the molecular bridges are identical. Finally, donor electronic state energies may differ from the work functions of metal electrodes. As such, different CT energy barriers appear likely in D-B-A, M-B-A/D-B-M, and M-B-M structures. A quantitative fit of the framework developed here to the experimental data in Fig. 1 is expected to constrain the CT barriers and decoherence values, and analysis of such fits will be presented elsewhere.

In summary, we have developed a theoretical framework to compute CT rates and molecular conductances without assuming a transport mechanism *a priori*. This approach reveals that a non-linear correlation exists between rates and conductances. The non-linearity arises from CT energy barrier and decoherence differences in the experiments. A decrease in the CT energy barrier and/or an increase in the decoherence rate shifts the position of the crossover from exponential to a weaker distance dependence of rates and conductances. In fact, by manipulating the CT energy barriers and bridge decoherence, a wide range of power law correlations can be accessed among CT rates and molecular conductances. This theoretical framework explains the observed non-linear rate-conductance relationships evident in experimental data.

AUTHOR INFORMATION

Corresponding Authors

*Ravindra Venkatramani, Email: ravi.venkatramani@tifr.res.in

*David H. Waldeck, Email: dave@pitt.edu

*David N. Beratan, Email: david.beratan@duke.edu

Acknowledgements

R.V. acknowledges financial support from Tata Institute of Fundamental Research (Department of Atomic Energy, India). The authors gratefully acknowledge support from the National Science Foundation (CHE 1057953 to D.N.B., CHE 1057981 to D.H.W.).

REFERENCES

1. Nitzan, A. *J. Phys. Chem. A* **2001,** 105, (12), 2677-2679.
2. Nitzan, A. *Isr. J. Chem.* **2002,** 42, (2-3), 163-166.
3. Berlin, Y. A.; Ratner, M. A. *Radiat. Phys. Chem.* **2005,** 74, (3-4), 124-131.
4. Traub, M. C.; Brunschwig, B. S.; Lewis, N. S. *J. Phys. Chem. B* **2007,** 111, (24), 6676-6683.
5. Schuster, G. B., *Long-Range Charge Transfer in DNA I and II*. Springer: Berlin, 2004; Vol. 236-237.
6. Davis, W. B.; Wasielewski, M. R.; Ratner, M. A.; Mujica, V.; Nitzan, A. *J. Phys. Chem. A* **1997,** 101, (35), 6158-6164.
7. Lewis, F. D.; Wu, T. F.; Zhang, Y. F.; Letsinger, R. L.; Greenfield, S. R.; Wasielewski, M. R. *Science* **1997,** 277, (5326), 673-676.
8. Berlin, Y. A.; Kurnikov, I. V.; Beratan, D.; Ratner, M. A.; Burin, A. L., DNA electron transfer processes: Some theoretical notions. In *Long-Range Charge Transfer in DNA Ii*, Springer-Verlag Berlin: Berlin, 2004; Vol. 237, pp 1-36.
9. Lewis, F. D.; Liu, J. Q.; Weigel, W.; Rettig, W.; Kurnikov, I. V.; Beratan, D. N. *Proc. Natl. Acad. Sci. U. S. A.* **2002,** 99, (20), 12536-12541.
10. Smalley, J. F.; Finklea, H. O.; Chidsey, C. E.; Linford, M. R.; Creager, S. E.; Ferraris, J. P.; Chalfant, K.; Zawodzinsk, T.; Feldberg, S. W.; Newton, M. D. *J. Am. Chem. Soc.* **2003,** 125, (7), 2004-13.
11. Paul, A.; Watson, R. M.; Wierzbinski, E.; Davis, K. L.; Sha, A.; Achim, C.; Waldeck, D. H. *J. Phys. Chem. B* **2010,** 114, (45), 14140-14148.
12. Paul, A.; Watson, R. M.; Lund, P.; Xing, Y. J.; Burke, K.; He, Y. F.; Borguet, E.; Achim, C.; Waldeck, D. H. *J. Phys. Chem. C* **2008,** 112, (18), 7233-7240.
13. Smalley, J. F.; Feldberg, S. W.; Chidsey, C. E. D.; Linford, M. R.; Newton, M. D.; Liu, Y. P. *J. Phys. Chem.* **1995,** 99, (35), 13141-13149.
14. He, J.; Sankey, O.; Lee, M.; Tao, N. J.; Li, X. L.; Lindsay, S. *Faraday Discuss.* **2006,** 131, 145-154.

15. Porath, D.; Bezryadin, A.; de Vries, S.; Dekker, C. *Nature* **2000,** 403, (6770), 635-638.
16. Cohen, H.; Nogues, C.; Ullien, D.; Daube, S.; Naaman, R.; Porath, D. *Faraday Discuss.* **2006,** 131, 367-376.
17. Guo, X. F.; Gorodetsky, A. A.; Hone, J.; Barton, J. K.; Nuckolls, C. *Nat. Nanotechnol.* **2008,** 3, (3), 163-167.
18. Tivanski, A. V.; He, Y. F.; Borguet, E.; Liu, H. Y.; Walker, G. C.; Waldeck, D. H. *J. Phys. Chem. B* **2005,** 109, (12), 5398-5402.
19. Li, C.; Pobelov, I.; Wandlowski, T.; Bagrets, A.; Arnold, A.; Evers, F. *J. Am. Chem. Soc.* **2008,** 130, 318-326.
20. Wierzbinski, E.; Venkatramani, R.; Davis, K. L.; Bezer, S.; Kong, J.; Xing, Y.; Borguet, E.; Achim, C.; Beratan, D. N.; Waldeck, D. H. *ACS Nano* **2013,** 7, (6), 5391-5401.
21. Segal, D.; Nitzan, A.; Davis, W. B.; Wasielewski, M. R.; Ratner, M. A. *J. Phys. Chem. B* **2000,** 104, (16), 3817-3829.
22. Segal, D.; Nitzan, A.; Ratner, M.; Davis, W. B. *J. Phys. Chem. B* **2000,** 104, (13), 2790-2793.
23. Beratan, D. N.; Skourtis, S. S.; Balabin, I. A.; Balaeff, A.; Keinan, S.; Venkatramani, R.; Xiao, D. Q. *Acc. Chem. Res.* **2009,** 42, (10), 1669-1678.
24. Skourtis, S. S.; Waldeck, D. H.; Beratan, D. N. *Annu. Rev. Phys. Chem.* **2010,** 61, 461-485.
25. Venkatramani, R.; Keinan, S.; Balaeff, A.; Beratan, D. N. *Coord. Chem. Rev.* **2011,** 255, 635-658.
26. Felts, A. K.; Pollard, W. T.; Friesner, R. A. *J. Phys. Chem.* **1995,** 99, (9), 2929-2940.
27. Okada, A.; Chernyak, V.; Mukamel, S. *J. Phys. Chem. A* **1998,** 102, (8), 1241-1251.
28. Yeganeh, S.; Ratner, M. A.; Mujica, V. *J. Chem. Phys.* **2007,** 126, (16).
29. Skourtis, S.; Nitzan, A. *J. Chem. Phys.* **2003,** 119, (12), 6271-6276.
30. Skourtis, S. S.; Beratan, D. N.; Naaman, R.; Nitzan, A.; Waldeck, D. H. *Phys. Rev. Lett.* **2008,** 101, (23).
31. Skourtis, S. S.; Dasilva, A. J. R.; Bialek, W.; Onuchic, J. N. *J. Phys. Chem.* **1992,** 96, (20), 8034-8041.
32. Marcus, R. A.; Sutin, N. *Biochim. Biophys. Acta* **1985,** 811, (3), 265-322.
33. Lowdin, P. O. *J Math Phys* **1962,** 3, (5), 969-&.
34. Larsson, S. *J. Am. Chem. Soc.* **1981,** 103, (14), 4034-4040.
35. Larsson, S. *J Chem Soc Farad T 2* **1983,** 79, 1375-1388.
36. Mishra, A. K.; Waldeck, D. H. *J. Phys. Chem. C* **2011,** 115, (42), 20662-20673.
37. Napper, A. M.; Liu, H. Y.; Waldeck, D. H. *J. Phys. Chem. B* **2001,** 105, (32), 7699-7707.
38. Datta, S., *Quantum Transport: Atom to Transistor*. Cambridge University Press: 2005.
39. Datta, S., *Electronic transport in mesoscopic systems*. Cambridge University Press: Cambridge, 1997.
40. Maassen, J.; Zahid, F.; Guo, H. *Physical Review B* **2009,** 80, (12).
41. Galperin, M.; Nitzan, A.; Ratner, M. A. *Physical Review B* **2006,** 74, (7).
42. Hartle, R.; Volkovich, R.; Thoss, M.; Peskin, U. *J. Chem. Phys.* **2010,** 133, (8).
43. Lykkebo, J.; Gagliardi, A.; Pecchia, A.; Solomon, G. C. *ACS Nano* **2013,** 7, (10), 9183-9194.
44. Bixon, M.; Jortner, J. *Chem. Phys.* **2002,** 281, (2-3), 393-408.
45. Venkatramani, R.; Davis, K. L.; Wierzbinski, E.; Bezer, S.; Balaeff, A.; Keinan, S.; Paul, A.; Kocsis, L.; Beratan, D. N.; Achim, C.; Waldeck, D. H. *J. Am. Chem. Soc.* **2011,** 133, 62-72.

46. McConnell, H. *J. Chem. Phys.* **1961,** 35, (2), 508-515.
47. Onuchic, J. N.; Beratan, D. N. *J. Am. Chem. Soc.* **1987,** 109, (22), 6771-6778.
48. Xing, Y.; Park, T. H.; Venkatramani, R.; Keinan, S.; Beratan, D. N.; Therien, M. J.; Borguet, E. *J. Am. Chem. Soc.* **2010,** 132, (23), 7946-7956.
49. Berlin, Y. A.; Burin, A. L.; Ratner, M. A. *Chem. Phys.* **2002,** 275, (1-3), 61-74.
50. Kubatkin, S.; Danilov, A.; Hjort, M.; Cornil, J.; Bredas, J. L.; Stuhr-Hansen, N.; Hedegard, P.; Bjornholm, T. *Nature* **2003,** 425, (6959), 698-701.
51. Neaton, J. B.; Hybertsen, M. S.; Louie, S. G. *Phys. Rev. Lett.* **2006,** 97, (21).